Table 1 Payload mass delivered for a range of trip times

Trip time (days)	350	300	250
a_c^f, mm s^{-2}	1.60	2.59	4.97
a_c^c, mm s^{-2}	1.10	1.72	3.01
σ_s, g m^{-2}	3.5	2.5	1.5
m_T, kg	375	375	375
m_p^f, kg	144.7	108.9	68.5
m_p^c, kg			
$\kappa = 0.1$	200.9	180.9	170.8
$\kappa = 0.2$	185.0	163.2	152.2
Δm_p, kg			
$\kappa = 0.1$	56.1	71.0	102.3
$\kappa = 0.2$	40.3	54.3	83.8
κ^*	0.45	0.51	0.65

has the same properties as the flat sail. However, a penalty will be added to account for the additional mass required for the director mirror. Therefore, the assembly loading of the compound solar sail will be defined as $\sigma_s(1 + \kappa)$, for some mass penalty κ. The payload mass of the compound solar sail may then be written in terms of the total mass as

$$m_p^c = \left[1 - (1 + \kappa)\left(\sigma_s a_c^c \big/ 2P_0\right)\right] m_T \tag{11}$$

where the superscript c refers to a compound solar sail.

For a given trip time, the compound solar sail will in general be able to deliver a larger payload mass fraction than a flat solar sail. However, as the mass penalty for the compound solar sail increases the difference in payload mass fraction will of course fall. The break-even mass penalty κ^*, where both solar sails deliver the same payload mass, can be obtained by equating the payload masses defined by Eq. (10) and (11) to obtain

$$\kappa^* = a_c^f \big/ a_c^c - 1 \tag{12}$$

To provide an evaluation of the flat and compound solar sail, the payload mass delivered to Mars will be determined for a fixed launch mass of 375 kg, corresponding to the approximate $C_3 = 0$ capacity of the Taurus XL launch vehicle.

The delivered payload mass and increase in payload mass Δm_p have been determined for a range of trip times, as shown in Table 1. For the compound solar sail, a fixed mass penalty of 0.1 and 0.2 has been assumed. It can be seen that the benefit of the compound solar sail for long trip times of order 350 days is quite modest, corresponding to a 30% increase in delivered payload for a compound solar sail mass penalty of 0.2. However, for fast trip times of order 250 days, the benefit of the compound solar sail is more significant. Again, for a mass penalty of 0.2, the payload delivered by the compound solar sail is more than doubled. In this case the compound solar sail delivers a greater payload mass for a mass penalty of up to 0.65.

IV. Conclusions

A simple coplanar transfer problem has been used to derive a minimum-time steering law for a compound solar sail. It has been shown that, in principle, a compound solar sail can deliver a significantly greater payload mass fraction than a flat solar sail for short-trip times. Because the compound solar sail has not undergone the same level of detailed design that flat solar sails have, it remains to be seen whether mass penalties as low as 0.2 could be achieved in practice. If such configurations are possible, compound solar sails offer significant benefits for future fast missions.

References

[1]McInnes, C. R., *Solar Sailing: Technology, Dynamics and Mission Applications*, Springer–Praxis Series in Space Science and Technology, Springer-Verlag, Berlin, 1999, pp. 32–55.

[2]Malanin, V. V., and Repyakh, A. V., "On the Motion of a Craft with Two Solar Sails," *Problemy Mekhaniki Upravlyayemogo Dvizheniya*, No. 5, 1974, pp. 99–108.

[3]Forward, R. L., "Solar Photon Thrustor," *Journal of Spacecraft and Rockets*, Vol. 27, No. 4, 1990, pp. 411–416.

[4]Wood, L. J., Bauer, T. P., and Zondervan, K. P., "Comment on 'Time-Optimal Orbit Transfer Trajectory for Solar Sail Spacecraft,'" *Journal of Guidance and Control*, Vol. 5, No. 2, 1982, pp. 221–224.

Collision Dynamics for Space Tethers

Chris Blanksby* and Pavel Trivailo†
Royal Melbourne Institute of Technology, Melbourne, Victoria 3001, Australia

Introduction

OPERATION of tethers from large space structures such as the Space Shuttle Orbiter and, in the near future, the International Space Station (ISS) raises the possibility of collisions between the tether and parts of the structure. Such collisions could occur as a result of unstable retrieval, severance of the tether (and subsequent recoil), impact with space debris, or various other unscheduled events. The behavior of the system during such an event has not been considered in the literature, to the best of the authors' knowledge. An understanding of the dynamics of such an event is considered important in the development of contingency measures for minimizing risk.

This Note presents a methodology developed to examine the collision event. Numerical simulation results showing the details of a potential collision event involving the ISS are also presented.

For the purposes of this study, a lumped-mass model of the system is employed. As has been recognized in a number of papers,[1–4] the lumped-mass model is better able to deal with high curvature of the tether. This functionality is necessary to model the collision event, which would typically occur after the advent of extreme tether motion.

Theory

Tether Dynamics

The tether dynamics model uses a series of $n + 1$ lumped masses, connected together by n segments with linear stiffness, to represent the tether and is similar to that developed by Banerjee[4] or Banerjee and Do.[3] Some differences to these models exist in the application of Kane's equations to the system and in the means employed for deploying and retrieving the tether. The formulation of the equations of motion is such that they can be classified as Order-N, i.e., the computational effort required to solve for the acceleration vector of each body varies linearly with the number of bodies. Previous validations have shown the accuracy of the model to be within 5% for a range of situations.[5]

Environmental and system contributions to generalized forces included in the model are 1) gravitational force, 2) tether tension force, 3) electromagnetic force, 4) internal damping force, 5) aerodynamic force, and 6) arbitrary, applied force.

Collision

The model just described above has been enhanced to enable collisions to be modeled. In the present implementation only collisions between the tether and the space structure are considered; collisions between different segments of the tether are ignored. For the purposes of identifying locations of collisions, the space structure

Received 13 September 1999; revision received 22 May 2000; accepted for publication 26 July 2000.

*Doctoral Student, Department of Aerospace Engineering, GPO Box 2476V.

†Associate Professor, Department of Aerospace Engineering, GPO Box 2476V.

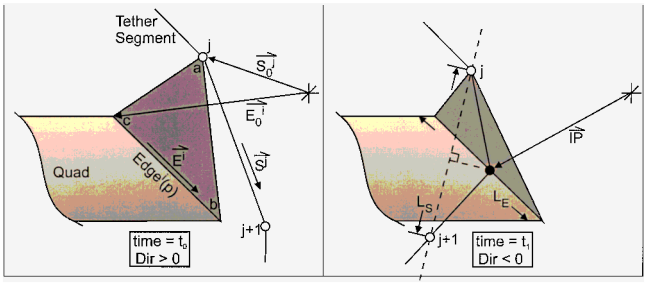

Fig. 1 Collision modeling parameters.

is modeled as a series of quads (flat, four-sided elements). Each quad has four edges, which are used to determine if a collision has occurred and to locate its coordinates.

Two distinct phases of a collision are considered: the occurrence of the collision and the motion following collision. Occurrence of a collision is detected in the following way:

Prescribe the line representing the edge i of the quad as

$$\mathbf{Edge}^i(p) = \boldsymbol{E}_0^i + \boldsymbol{E}^i \cdot p, \qquad (i = 1, 2, 3, 4) \tag{1}$$

where $\boldsymbol{E}_0^i$ and $\boldsymbol{E}^i$ are defined in Fig. 1 and p is the distance along the edge from $\boldsymbol{E}_0^i$ in the direction of $\boldsymbol{E}^i$.

Prescribe the line representing the segment j of the tether as

$$\mathbf{Seg}^j(q) = \boldsymbol{S}_0^j + \boldsymbol{S}^j \cdot q, \qquad (j = 1, \ldots, n) \tag{2}$$

where $\boldsymbol{S}_0^j$ and $\boldsymbol{S}^j$ are defined in Fig. 1 and q is the distance along the segment from $\boldsymbol{S}_0^j$ in the direction of $\boldsymbol{S}^i$.

The position of the segment relative to the edge (i.e., which side of the edge the segment is on) is found by evaluating the dot product between $\boldsymbol{S}^j$ and the normal to the plane a, b, c shown in Fig. 1. This can be expressed as

$$\mathrm{Dir} = \left[\mathbf{Edge}^i(L_E) - \mathbf{Seg}^j(0)\right] \times [\mathbf{Edge}^i(0) - \mathbf{Seg}^j(0)] \cdot \left[\mathbf{Seg}^j(L_S) - \mathbf{Seg}^j(0)\right], \qquad (i = 1, 2, 3, 4;\ j = 1, \ldots, n) \tag{3}$$

where L_S is the length of the segment and L_E is the length of the edge.

By monitoring the value of Dir from one time step to the next, a change in sign can be detected indicating that the two lines (segment and edge) have crossed. The coordinates of the intersection point $\boldsymbol{IP}$ are approximated as the point on the edge that is the minimum distance from any point on the crossing segment:

$$\mathrm{Distance} = |\mathbf{Seg}^j(q) - \mathbf{Edge}^i(p)| \qquad (i = 1, 2, 3, 4;\ j = 1, \ldots, n) \tag{4}$$

To minimize the distance, let

$$\frac{\partial \mathrm{Distance}}{\partial p} = 0, \qquad \frac{\partial \mathrm{Distance}}{\partial q} = 0 \tag{5}$$

Solving for the parameter p gives the location for the intersection on the edge.

$$p = \frac{(\boldsymbol{S}^j \times \boldsymbol{E}^i) \cdot \left(\boldsymbol{E}_0^i \times \boldsymbol{S}^j\right) - (\boldsymbol{S}^j \times \boldsymbol{E}^i) \cdot \left(\boldsymbol{S}_0^j \times \boldsymbol{S}^j\right)}{|\boldsymbol{S}^j \times \boldsymbol{E}^i|^2} \qquad (i = 1, 2, 3, 4;\ j = 1, \ldots, n) \tag{6}$$

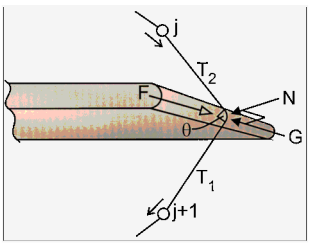

Fig. 2 Friction effects modeling parameters.

$$\Rightarrow \boldsymbol{IP} = \boldsymbol{E}_0 + \boldsymbol{E} \cdot \frac{(\boldsymbol{S}^j \times \boldsymbol{E}^i) \cdot \left(\boldsymbol{E}_0^i \times \boldsymbol{S}^j\right) - (\boldsymbol{S}^j \times \boldsymbol{E}^i) \cdot \left(\boldsymbol{S}_0^j \times \boldsymbol{S}^j\right)}{|\boldsymbol{S}^j \times \boldsymbol{E}^i|^2} \qquad (i = 1, 2, 3, 4;\ j = 1, \ldots, n) \tag{7}$$

This is an approximation as the true intersection point will also depend on the velocity of the segment and its position at the preceding time step. The full solution is, however, considerably more complex and would significantly increase computational time while providing only a very small increase in accuracy.

Finally, check that the coordinates of the intersection point are within the bounds of both the segment and the edge:

$$[\mathbf{Edge}(0) - \boldsymbol{IP}] \cdot [\mathbf{Edge}(L_E) - \boldsymbol{IP}] > 0 \tag{8}$$

$$[\mathbf{Seg}(0) - \boldsymbol{IP}] \cdot [\mathbf{Seg}(L_S) - \boldsymbol{IP}] > 0 \tag{9}$$

Having detected and located a collision, the simulation must be modified to model accurately the new system. This is achieved by adjusting direction of the spring force generated by tether elasticity so that tension is directed toward the intersection point. The magnitude of the spring force is adjusted using revised tension based on friction effects as discussed next.

Friction Effects

The effects of friction between the edge of the quad and the segment are incorporated in the model. The effects of friction are twofold. First they determine the magnitude of the tension in the segment on either side of the intersection, and second they determine how the tether segment slips sideways along an edge. Parameters for both effects are given in Fig. 2. These two effects are modeled separately. The magnitude of the tension on either side of the intersection is significantly influenced by the local geometry of the edge. For simplicity in this analysis, it is assumed that the geometry of the edge is a constant radius curve (see Fig. 2). This assumption permits the use of the Euler formula for belt friction around a pulley:

$$T_1/T_2 = e^{\mu\theta} \tag{10}$$

where μ (>0) is the friction coefficient between the surfaces, θ (>0) is the angle of lap, and T_1 and T_2 are the tension in the segment on either side of the edge ($T_1 > T_2$) (local variation in tension over the edge is ignored).

The values of T_1 and T_2 can be determined by the linear elastic and compatibility relationships in Eqs. (11–13):

$$T_1 = EA[SL_1/UL_1 - 1] \tag{11}$$

$$T_2 = EA[SL_2/UL_2 - 1] \tag{12}$$

$$UL_1 + UL_2 = UL \tag{13}$$

where SL_1 and SL_2 are the stretched lengths of the tether segment corresponding to T_1 and T_2, UL_1 and UL_2 are the unstretched lengths of the tether segment corresponding to T_1 and T_2, UL is the total unstretched length of the tether segment, and EA is the tether stiffness.

Solution of Eqs. (11–13) for tension in the segment on either side of the intersection yields

$$T2 = \frac{EASL_1}{2ULe^{\mu\theta}} + \frac{EASL_2}{2UL} - \frac{EA}{2} - \frac{EA}{2e^{\mu\theta}} + \cdots \frac{EA}{2}\sqrt{(UL - SL_2)^2 e^{2\mu\theta} - 2\left[UL^2 - (SL_1 + SL_2)UL - SL_1SL_2\right]e^{\mu\theta} + (UL - SL_1)^2} \tag{14}$$

$$T1 = T2e^{\mu\theta} \tag{15}$$

In the formulation thus far, no specification has been made as to which side of the intersection has the greater tension ($T_1 > T_2$). Because surface friction must oppose the direction of motion, the greater tension T_1 must occur in the part of the segment with the greatest motion away from the edge. The lower tension T_2 must therefore occur in the part of the segment that has the greatest movement toward the edge.

The second effect of friction, slippage of a segment sideways along an edge, is determined by calculating a normal force $\boldsymbol{N}$ and side force $\boldsymbol{G}$, caused by the collision, and then relocating the coordinates of the collision to place the system in equilibrium. For the case where the tether slides in the positive direction across the edge, the process is as follows:

Prescribe the resultant force $\boldsymbol{R}$ of the tether on the edge:

$$\boldsymbol{R} = \left[\frac{\mathbf{Seg}^j(L) - \boldsymbol{IP}}{|\mathbf{Seg}^j(L) - \boldsymbol{IP}|} T_1 + \frac{\mathbf{Seg}^j(L) - \boldsymbol{IP}}{|\mathbf{Seg}^j(0) - \boldsymbol{IP}|} T_2 \right] \qquad (j = 1, \ldots, n) \tag{16}$$

Calculate the side force $\boldsymbol{G}$ and the normal force $\boldsymbol{N}$:

$$\boldsymbol{G} = (\boldsymbol{R} \cdot \hat{\boldsymbol{E}}^i)\hat{\boldsymbol{E}}^i \tag{17}$$

$$\boldsymbol{N} = \boldsymbol{R} - \boldsymbol{G} \tag{18}$$

Finally calculate the friction force $\boldsymbol{F}$:

$$\boldsymbol{F} = -|\mu N|\hat{\boldsymbol{G}} \tag{19}$$

Placement is determined by moving the intersection point $\boldsymbol{IP}$ along the edge until the side force $\boldsymbol{G}$ is less than the friction force $\boldsymbol{F}$. These friction models do not account for the inertia of the tether segment, which is assumed to be small.

The model also incorporates the technology to release a collision when appropriate. This may occur, for example, if the tether reverses its swing or if the tether slides off an edge. The method for detecting a release is essentially the same as for detecting a collision.

Additional Features

One further feature of the collision model accounts for the special case, where the motion of a lumped mass at the end of a segment causes it to collide with the center of a quad. The model detailed thus far does not account for this case and would allow the lumped mass to pass through the quad. The system must be monitored for such collisions. To do this, the projected position of the lumped mass onto the quad $\boldsymbol{P}$ along a line normal to the quad is calculated.

$$\boldsymbol{P} = \frac{d - \hat{\boldsymbol{M}} \cdot \boldsymbol{LM}}{\hat{\boldsymbol{M}}^2} \tag{20}$$

where $\boldsymbol{LM}$ is the position of the lumped mass, $\boldsymbol{M}$ is the quad normal, and $\boldsymbol{M} \cdot \boldsymbol{Q} = d$ where $\boldsymbol{Q}$ is any point on the quad.

The distance from the lumped mass to the quad is then given by

$$D = |\boldsymbol{LM} - \boldsymbol{P}| \tag{21}$$

Impact is said to have occurred if the distance $\boldsymbol{D}$ is less than a predefined thickness of the quad and if the point $\boldsymbol{P}$ on the quad is within the bounds of the quad.

When a collision is detected, the normal component of the velocity of the lumped mass, relative to the quad, is reversed, thus simulating rebound. A coefficient of restitution to simulate damping during the impact is also introduced into the equation:

$$\boldsymbol{V}_R = \boldsymbol{V}_I - \hat{\boldsymbol{M}}(\boldsymbol{V}_I \cdot \hat{\boldsymbol{M}})(1 + RC) \tag{22}$$

where $\boldsymbol{V}_R$ is the rebound velocity, $\boldsymbol{V}_I$ is the impact velocity, and $\boldsymbol{RC}$ is the coefficient of restitution ($0 < RC < 1$)

The modeling procedure described here can be easily extended to allow for multiple collisions on one segment and the sliding of an intersection point past a lumped mass. These features have been included the computer implementation of this model.

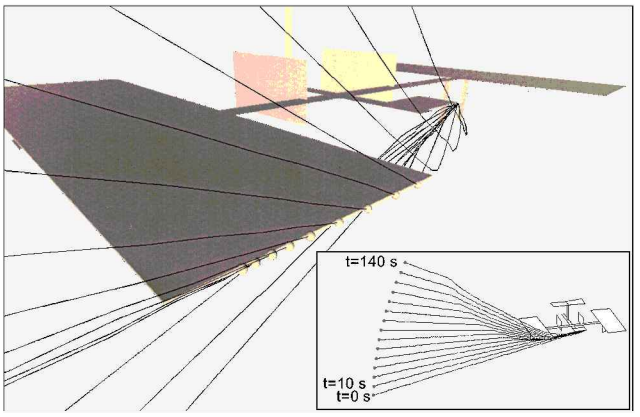

Fig. 3 Tether collision simulation (subsatellite attached).

Analysis

Simulation Cases

A number of cases have been identified where collisions between the tether and the structure of the ISS are possible; these include 1) excessive retrieval rate, 2) undamped skip-rope motion during retrieval, and 3) tether recoil (resulting from tether severance). Tether recoil is distinctly different from the other cases, as the subsatellite will not be attached to the tether (because the tether has severed). Because the subsatellite is no longer attached, the tether goes slack and recoil occurs very rapidly. It is therefore the most difficult collision case to prevent. Simulations have shown that entanglement of the ISS can occur in less than 40 s in this case.

A much simpler collision case where the subsatellite is attached to a short tether, which is swinging upward past the ISS (this could occur for various reasons, but could be easily prevented through intentional severance of the tether), is presented in Fig. 3. The following stages can be observed: 1) free tether; 2) tether intersection with solar panel; 3) tether slipping along solar panel, associated tether dynamics and rebound of the tether off the quad; and 4) tether slipping off the quad (release) and associated tether dynamics.

Discussion

The method presented for modeling the tether after a collision is superior to the introduction of a new node at the intersection point. Introduction of a new node would change the system properties significantly. In particular, constraint equations or forces would need to be added for the extra node. Also, the position of the new node would need to be continuously adjusted as the tether segment moves across the edge.

Results of the analysis clearly show that the algorithm described enables detection of collisions. More important, it allows the simulation to continue and the dynamics of the event to be studied. Simulations where the tether recoil occurs have shown that following severance the ISS can rapidly become entangled in the tether. However, because the subsatellite is not attached, the tension in the tether is low, and hence contact forces are also low. Entanglement can, however, still constitute significant hazard. Simulations where severance does not occur and the subsatellite is still attached show a much greater time before first contact. Higher contact forces also occur; however, prevention is relatively easily implemented via intentional severance of the tether at the ISS.

Conclusions

An algorithm for the detection and modeling of collisions between a space structure and a tether has been presented. This algorithm has been merged into a dynamic simulation package using a lumped-mass model for the tether. A simulation of a possible collision case involving the ISS has been presented using this model.

Further applications of this technique can include the study of tether dynamics during contact between the tether and the deployer mechanism or guide.

References

[1]Djerassi, S., and Bambeger, H., "Simultaneous Deployment of a Cable from Two Moving Platforms," *Journal of Guidance, Control, and Dynamics*, Vol. 21, No. 2, 1998, pp. 271–276.

[2]Kim, E., and Vadali, S. R., "Modelling Issues Related to Retrieval of Tethered Satellite Systems," *Journal of Guidance, Control, and Dynamics*, Vol. 18, No. 5, 1995, pp. 1169–1176.

[3]Banerjee, Arun K., and Do, Van N., "Deployment of a Cable Connecting a Ship to an Underwater Vehicle," *Journal of Guidance, Control, and Dynamics*, Vol. 17, No. 6, 1994, pp. 1327–1332.

[4]Banerjee, A. K., "Dynamics of Tethered Payloads with Deployment Rate Control," *Journal of Guidance, Control, and Dynamics*, Vol. 13, No. 4, 1990, pp. 759–761.

[5]Blanksby, C., and Trivailo, P., "Deployment/Retrieval, Earth's Magnetic Field Interaction and Tether Severance Modelling for the Tethered Satellite System," *Proceedings of the International Aerospace Congress 1997*, Vol. 1, Sydney, Australia, 1997, pp. 81–96.

Two Projectiles Connected by a Flexible Tether Dropped in the Atmosphere

Geoffrey Frost* and Mark Costello†
Oregon State University, Corvallis, Oregon 97331

Introduction

CONNECTING two bodies by means of a tether has been used in many aerospace applications including tethered spacecraft,[1,2] aircraft air refueling,[3,4] and atmospheric balloons.[5] More recently, designers have proposed weapon systems consisting of two projectiles connected by a tether line.[6] In these concepts the lead projectile is generally a bomb, and the follower projectile is a sensor platform. The ordnance is released from an aircraft at altitude and drops toward a target on the ground. Initially, the two projectiles are rigidly attached. At a prespecified time the projectiles separate and subsequently unreel the tether line. After the tether line is fully payed out, the system settles toward a steady state as it approaches the ground. Maximum tether line loads usually occur shortly after the tether is fully deployed. This time instant is defined as the *snatch* point. Snatch loads are typically large, to the point where line failure is an important concern. Designers must balance the need to unreel the tether line in a specified period of time while at the same time limiting tether line loads, follower projectile acceleration, and lead projectile trajectory deviations. Previous work by Frost and Costello[7] developed a dynamic model suitable for simulating the exterior ballistics of this weapon system from release of the weapon to impact on the ground. Here, we use this dynamic model to establish how primary system design parameters such as projectile mass ratio, drag coefficient ratio, and tether stiffness affect performance of the weapon.

Dynamic Model Description

Both the lead and follower projectiles are modeled as point masses, and the tether line is likewise discretized as an open chain of point masses, or beads, where adjacent mass elements are connected by a spring and damper in parallel. Each bead has three translational degrees of freedom. The projectiles and tether beads are acted upon by gravitational, aerodynamic, and elastic forces. The Earth's surface is used as an inertial reference frame. Air density is computed using the standard atmosphere model.[8] The projectile drag coefficients are Mach-number dependent and are computed by linear interpolation of tabulated data. Aerodynamic forces on the tether line include skin-friction drag along the tether line and flat-plate drag perpendicular to the tether line. As the lead and follower projectiles separate, the tether line pays out. There are two aspects to modeling this process, namely, the pay out of the tether line from the lead projectile and the motion of released tether line. The tether deployment model initially places all tether beads on the lead projectile. As the tether line is payed out, beads are released from the lead projectile into the atmosphere. A bead is not placed into the atmosphere until a sufficient length of line has been unreeled. For this reason, during deployment only a fraction of the tether beads are dynamically active in the atmosphere. When a bead is placed into the atmosphere, it is placed along the line from the release point to the last bead released, and initial conditions are established such that the elastic force across the line is unchanged. This tends to prevent a discontinuity in the tether line out rate as a result of bead release. However, because aerodynamic forces act on the bead immediately after it is released, a slight perturbation is generally observed when a tether bead is released. When a bead is released, the mass of the lead projectile is reduced by the released bead weight; the length from the release point to the last tether bead released is reset along with the stiffness and damping coefficients of the exiting tether line. The elastic force between the lead object and the neighboring bead acts on the reel to pay out the tether line. When the full length of tether line has been unspooled, the acceleration and the velocity of the reel are set to zero.

Simulation Results

Typical values were selected for a generic 2000-lbf (8896.44 N) bomb lead projectile released from a parent aircraft and a follower projectile, which is a sensor platform. The lead projectile is released from the parent aircraft at an altitude of 25,000 ft (7620 m) and a speed of 500 ft/s (152.4 m/s). The lead projectile reference area is 1.77 ft^2 (0.164 m^2). The follower projectile weighs 20 lbf (88.96 N) (1% of the lead projectile) and is released from the lead projectile at $t = 0$ s. The tether line has the following properties: length = 1000 ft (304.8 m), weight per unit length = 0.01 lbf/ft (0.146 N/m), diameter = 0.0082 ft (0.0025 m), stiffness = 62,500 lbf·ft/ft (278,013 N-m/m), skin-friction drag coefficient = 0.007, and flat-plate drag coefficient = 1.1. The tether reel weighs 5 lbf (2.24 N). All simulation results use 100 beads to discretize the tether line.

The separation dynamics are driven in large part by the difference between the drag forces on the lead and follower projectiles. Figure 1 plots the range of the lead and follower projectiles for five different follower-to-lead drag coefficient ratios (1.25, 1.50, 1.75, 2.00, and 5.00). The shape of the drag coefficient curve vs Mach number is identical for both projectiles. As would be expected, a decrease in range is noticed when the drag coefficient ratio is increased. One of the primary questions designers are faced with is how to shape the follower projectile to unreel the tether line over a specified duration of time while at the same time limiting the tether line maximum loads and the follower projectile acceleration at the snatch point. Figure 2 shows the length of tether line deployed from the lead projectile over the trajectory for different drag coefficient ratios. Figure 3 plots the magnitude of the inertial velocity of the lead projectile. When the follower projectile drag coefficient is increased relative to the lead projectile, the tether line pays out more rapidly so that tether line tension acting on the lead projectile is higher over a longer portion of the trajectory, contributing to a decrease in range. For a drag coefficient ratio of 5.0, the decrease in range of 15% is substantial; however, the corresponding decrease in the tether deployment time of approximately 1 s is modest. For the configuration analyzed the steady-state drop velocity is larger than the release velocity so that the lead projectile increases its speed over the trajectory until it impacts the ground and its velocity goes

Received 17 September 1999; revision received 28 May 2000; accepted for publication 20 July 2000.

*Graduate Research Assistant, Department of Mechanical Engineering.

†Assistant Professor, Department of Mechanical Engineering. Member AIAA.